# CHAPTER 14

# CROSS-SHORE MOMENTUM FLUX DUE TO SHEAR INSTABILITIES

Ad Reniers[1] and Jurjen A. Battjes

## Abstract

Results obtained from a laboratory experiment on shear instabilities in wave-driven longshore currents were used to analyse the cross-shore structure of the shear instability induced momentum flux. As the shear instabilities grew in the downstream direction, a significant cross-shore momentum flux occurred. However, the expected changes in the mean longshore current velocity profile were not observed.

## Introduction

In spring 1994 an experiment on the generation of shear instabilities in wave-driven longshore currents was performed in a large wave basin. Shear instabilities were found to occur when using obliquely incident waves to create an alongshore uniform current over a barred beach (Reniers et al., 1994).

Shear instabilities are assumed to cause a cross-shore redistribution of mass and momentum in the surfzone. The redistribution depends on the cross-shore structure of the shear instabilities and the phase coupling between the horizontal velocity components. Numerical studies (Dodd and Thornton, 1990, 1993, Putrevu and Svendsen, 1992) indicate an inflection point in the redistribution of momentum, resulting in a smoothing of the initial longshore current velocity profile. These predictions can now be checked quantitatively.

First a brief layout of the experimental set-up is given. For a more detailed description reference is made to Reniers et al. (1996). Next proof is given of the existence of shear instabilities using a spectral analysis method (MEM) to obtain the frequency wave-number spectrum based on the fact that the shear instability signature is outside the gravity-wave range. This enables us

[1]Faculty of Civil Engineering, Delft University of Technology, P.O. Box 5048, Delft, The Netherlands, ad.reniers@wldelft.nl

to establish which energy corresponds to shear instabilities only. Phase coupling between the $u$ and $v$ velocity components results in cross-shore flux of momentum. This is examined in detail using cross-shore spectral analysis to compute the frequency distribution of the momentum flux induced by shear instabilities. The total transfer is obtained by integration over the frequency domain. The results are compared to the other terms in the longshore momentum equation used to compute the longshore current velocity.

## Experimental set-up

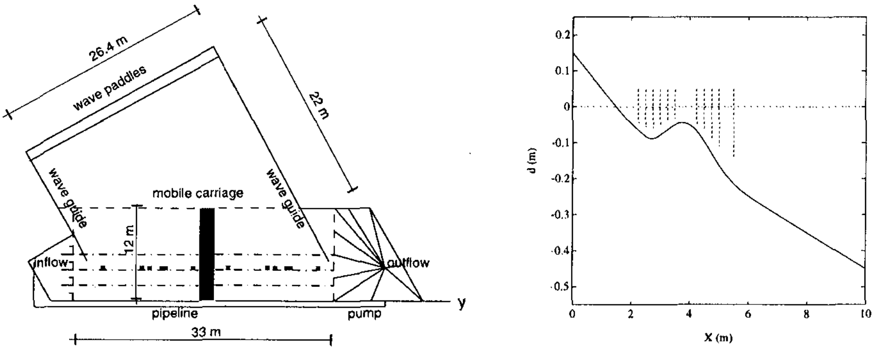


Figure 1: Left panel: plan view experimental set-up. Instrument positions of alongshore arrays indicated by the '*' signs. Right panel, bottom profile and deployment positions alongshore array indicated by the dashed lines.

The experimental set-up is shown in Figure 1. The left panel shows the plan view of the experimental layout. Incident waves are generated by a multi-paddle wave maker. Given the oblique alignment of the beach with respect to the wave maker the paddles could be operated in phase, generating longcrested waves. The longshore current generated by the waves breaking over the barred profile (right panel Figure 1) was recirculated using a pump system to prevent spurious recirculations in the basin (Visser, 1984, Reniers and Battjes, 1996). To further increase the alongshore uniformity the pumped discharge was redistributed at the inflow opening. The cross-shore distribution of the longshore current velocity profile was measured with instruments attached to the mobile carriage. Two alongshore arrays of six spatially lagged current velocity meters (see left panel Figure 1) were used to measure the velocities up-and downstream respectively and thus the alongshore development of the shear instabilities. Detailed measurements of the cross-shore structure for a particular wave condition, monochromatic waves with a wave height of 8 cm and a 1 s period, were obtained by repositioning the alongshore arrays perpendicular to the beach (see right panel Figure 1). During the repositioning the input wave and flow conditions were maintained. Measurements would restart after the disturbances induced by the repositioning of the instruments had disappeared (estimated duration less than half an hour). Note that instruments could not be positioned at the bar crest given the strong wave breaking induced turbulence.

**Shear instabilities**

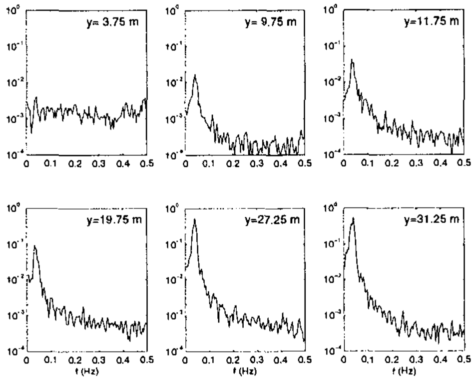


Figure 2: Alongshore development of low-frequency spectral density of alongshore velocity (m/s)2/Hz obtained from measurements at $x = 4.5$ m, from the inflow opening (upper left panel) to the outflow opening (lower right panel). Distance to the inflow opening given by $y$.

An example of the downstream development of the low-frequency spectrum of the alongshore velocity, measured with the two alongshore arrays positioned offshore of the bar ($x = 4.5$ m), is shown in Figure 2. It clearly shows the strong growth of the energy density in the 0 to .1 Hz frequency band. At this point it is not known whether energy in this frequency band corresponds to shear instabilities.

A spectral analysis technique based on maximum entropy was used to estimate the spectral distribution of energy density with alongshore wave number ($k_y$) of selected frequencies so as to determine which part of the energy density belonged to the shear instabilities (Reniers et al., 1996). Two results obtained at the downstream end of the basin, offshore of the bar and in the trough repsectively, are shown in Figure 3. The zero-mode edge-wave dispersion curve (for a plane beach) is also shown as a reference. It is obvious that all energy density is outside the gravity wave range indicated by the area below the edge wave dispersion line, i.e. belonging to shear instabilities only.

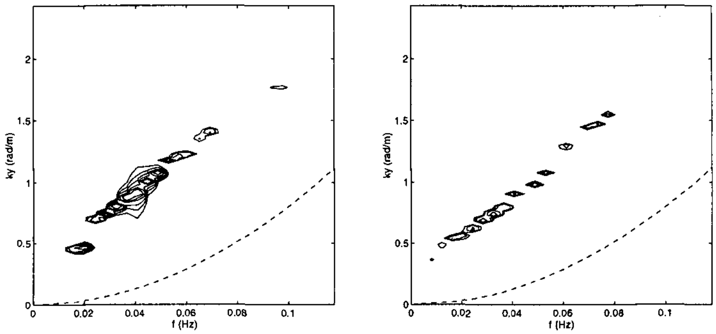


Figure 3: Left panel, $f - k_y$-spectrum at $x = 4.5m$. Right panel, $f - k_y$-spectrum at $x = 2.75m$. Zero-mode edge wave dispersion curve denoted by the dashed line.

From the almost linear dispersion lines of the shear instabilities it can be seen that the energy density propagates with approximately the same speed, $c = O(0.35)$ m/s, at both locations.

## Cross-shore momentum flux

The momentum flux at the cross-shore measurement locations, denoted by the subscript i, in a single transect may be obtained from:

$$R(x_i) = \rho d(x_i) < u(x_i, t)v(x_i, t) > \quad (1)$$

with $u$ and $v$ being the cross-shore and alongshore velocities associated with the shear instabilities, $<>$ denotes time averaging, $d$ the local water depth and $\rho$ the water density. The resulting flux depends on the spatial structure, mentioned in the previous paragraph, and the phase coupling between the velocity components. First we have a closer look at the frequency distribution of the momentum flux associated with the shear instabilities using cross-spectral analysis. To that end the velocity time series are written in Fourier series:

$$u(x_i, t) = \sum_n A_n e^{i\omega_n t} + * \quad (2)$$

$$v(x_i, t) = \sum_n B_n e^{i\omega_n t} + * \quad (3)$$

The momentum flux as function of frequency can be obtained from the co-spectral values:

$$R'(x_i,\omega_n) = d(x_i)(A_n B_n^* + A_n^* B_n)\delta\omega \tag{4}$$

The results of the frequency dependent momemtun flux at 27,25 m from the inflow opening is shown in Figure 4. The intermediate values have been obtained from linear interpolation in frequency and space. The flux is spatially concentrated at both sides of the bar crest ($x \simeq 3.75$ m), with maximum contributions around the peak shear instability frequency. At the shoreward side of the bar crest ($x < 3.75$ m) the momentum flux seems to be bimodal in frequency space. The frequency where the maximum flux is located decreases with increasing $x$-values, i.e. going further offshore, indicating that the higher frequencies, having smaller spatial scales, contribute less. The same can be seen going toward the shoreline, though to a lesser extent.

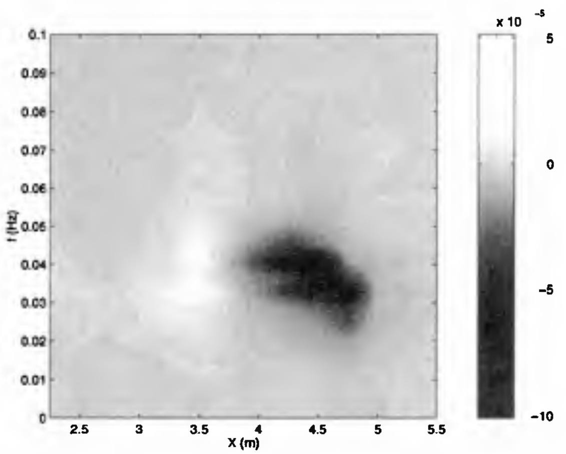


Figure 4: Frequency distribution of shear instability momentum flux, $R'$, at 27.25 m from the inflow opening expressed in $\frac{m^3}{s^2}$ rad/s

## Importance in longshore current modelling

For alongshore uniform steady state conditions the wave averaged longshore momentum equation is given by:

$$\frac{\partial S_{xy}}{\partial x} = \bar{\tau}_{y,b} \tag{5}$$

with the following contributions to the term on the left-hand side due to waves:

$$\frac{\partial}{\partial x}\rho\int_d \tilde{u}\tilde{v}\mathrm{d}z \tag{6}$$

turbulence:

$$\frac{\partial}{\partial x}\rho\int_d u'v'\mathrm{d}z = \rho\frac{\partial}{\partial x}\left(d\nu_t\frac{dV}{dx}\right) \tag{7}$$

and shear instabilities:

$$\frac{\partial}{\partial x}\rho\int_d uv\mathrm{d}z \tag{8}$$

which are balanced by the alongshore directed wave-averaged bottom shear stress given by the term on the right hand side. In the following the shear instability contribution is compared to the other components in the longshore momentum equation.

The total momentum flux due to the shear instabilities, $R$, is obtained by integrating $R'$ over all frequencies (see Figure 5). It shows the measured

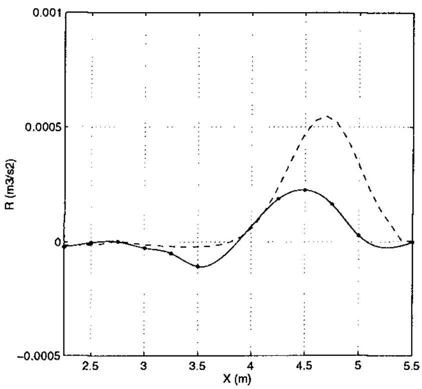


Figure 5: Total momentum transfer at y = 27.25 m from the inflow opening

flux, indicated by the dots, through which a spline has been fitted, in comparison to the horizontal mixing induced by wave breaking turbulence which is estimated from the measurements:

$$R_{\nu_t}(x) = d(x)\nu_t(x)\frac{dV}{dx} \tag{9}$$

using the measured longshore current velocity, $V$ and the measured wave height, $H$, as input. The turbulent eddy viscosity, $\nu_t$, is obtained from (Battjes, 1975):

$$\nu_t = H(x)\left(\frac{D(x)}{\rho}\right)^{\frac{1}{3}} \tag{10}$$

where the estimated wave dissipation is obtained from the measured wave transformation. It shows a significant contribution of the shear instabilities to the momentum flux at 27.25 m from the inflow opening, though almost everywhere smaller than the estimated horizontal mixing. The cross-shore profile of the momentum flux is not unlike results obtained from linear stability results (Church et al., 1992), though in this case the contribution in the trough seems to be considerably less. Given the fact that the shear instability intensity increases in the downstream direction the corresponding flux also evolves in this direction, which is apparent from the sequence of panels shown in Figure 6.

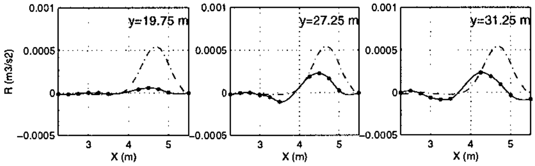


Figure 6: Alongshore development of total momentum transfer from the inflow opening (upper left panel) to the outflow opening (lower right panel). Distance to the inflow opening given by $y$.

At the upstream end of the basin little evidence of additional mixing is available, except in the very first panel in the upper left corner, which can be associated with the redistribution of the pumped discharge at the inflow opening. It takes until EMF07, located 19.75 m from the inflow opening, for the cross-shore momentum flux by shear instabilities to become evident.

After that a strong build-up is apparent, though never reaching values as indicated by the wave-breaking induced horizontal mixing. Note that the contribution in the trough stays small all along the beach.

Next we have a look at the cross-shore gradient of the mixing, using the spline, which contributes to the longshore momentum equation in computing the longshore current velocity profile:

$$F = \frac{\partial R}{\partial x} \tag{11}$$

The alongshore directed wave forcing, estimated from the measurements, is included as a reference:

$$F_w = \frac{\partial E_w sin(\theta)cos(\theta)}{\partial x} \tag{12}$$

where $E_w$ represents the wave energy (obtained from the measured wave transformation) and $\theta$ the angle of incidence (using Snell's law).

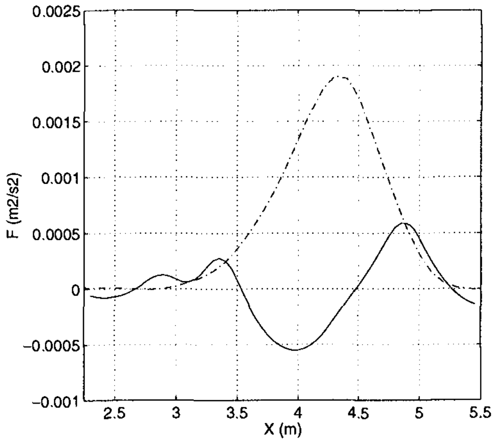


Figure 7: Contribution of shear instabilities to the longshore momentum balance at y = 27.25 m from the inflow opening (solid line). The alongshore-directed wave forcing is shown as a reference (dashed line)

The results at 27.25 m from the inflow opening, Figure 7, indicate a significant contribution to the longshore momentum balance. Based on this, it is expected that the maximum current velocity will decrease, given the opposite signs of the contribution by the shear instabilities and wave forcing at the bar crest. Furthermore, the shear instability contribution at the seaward side of the bar indicates a broadening of the longshore current velocity. Only minor differences in the current velocity over the trough are expected to occur.

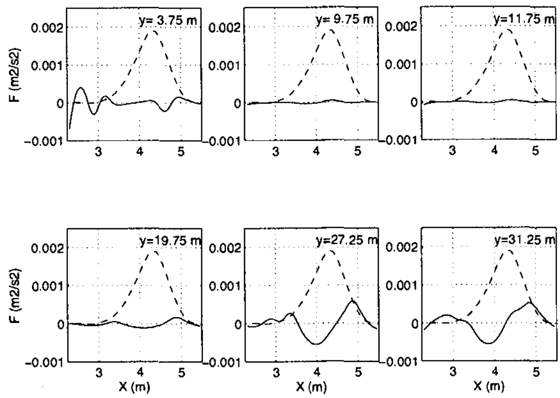


Figure 8: Alongshore development of shear instability contribution to longshore momentum balance (solid lines) from the inflow opening (upper left panel) to the outflow opening (lower right panel). The alongshore-directed wave forcing is shown as a reference (dashed lines)

The alongshore development of the shear instability contribution to the longshore momentum (see Figure 8) is in line with the results previously shown for the momentum flux. In all cases the contribution is considerably smaller than the alongshore directed wave forcing. It is worth to note that the development of the shear instability contribution to the longshore momentum balance stays small in the trough.

Finally we have a look at the measured development of the longshore current velocity (see Figure 9). There is no clear evidence of the effects of the shear instability induced cross-shore mixing on the alongshore development of the mean longshore current velocity profile.

## Conclusions

A detailed analysis of the cross-shore momentum flux due to the presence of finite amplitude shear instabilities in a wave-driven longshore current was made based on the measurents obtained during a laboratory experiment.

It showed an alongshore increasing cross-shore flux, becoming of compa-

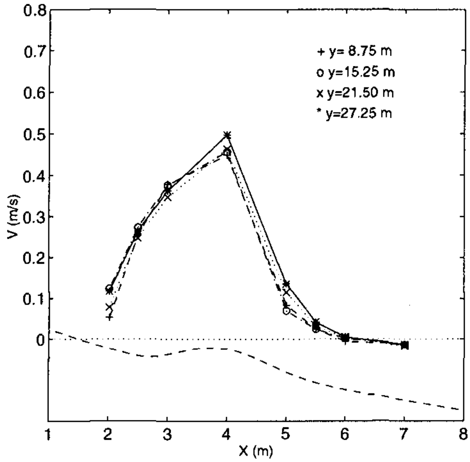


Figure 9: Longshore current velocity at four different transsects

rable order as the mixing associated with breaking wave induced turbulence at the downstream end of the basin.

However, no significant downstream changes in the mean longshore current velocity profile were detected. This can be explained by the fact that the shear instabilities take only effect near the outflow openening, whereas the wave forcing is present all along the beach.

*Acknowledgements.* The experiments, performed in the large multidirectional wave-basin at Delft Hydraulics, were funded by the European Community in the framework of the European Large Installations Plan (LIP), project 19 M. Ad Reniers was funded by the J.M. Burgers Centre for Fluid Mechanics in Delft.

## References

Battjes, J.A., 1975: Modelling of turbulence in the surfzone. Proc. Symp. Model. Techniques, San Francisco, pp. 1050-1061.

Church C.C., E.B. Thornton and J. Oltman-Shay, 1992: Mixing by shear instabilities of the longshore current. Proc. 23rd Int. Conf. Coastal Eng., Venice, pp. 2,999:3,011.

Dodd, N. and E.B. Thornton, 1990: Growth and energetics of shear waves in the nearshore. J.Geophys.Res., 95, C9, pp. 16,075:16,083.

Dodd, N. and E.B. Thornton, 1993: Longhore current instabilities: growth to finite amplitude. Proc. 23rd Int. Conf. Coastal Eng., Venice, pp. 2655-2668.

Putrevu, U and I.A. Svendsen,1992: Shear instability of longshore currents: A numerical study, J.Geophys. Res., 97, C5, pp. 7283-7303.

Reniers, A.J.H.M., J.A. Battjes, A. Falques and D.A. Huntley, 1994: Shear wave laboratory experiment. Proceedings IAHR waves conference, Vancouver, Canada, pp. 356-365.

Reniers, A.J.H.M., and J.A. Battjes, 1996: A laboratory study of longshore currents over barred and non-barred beaches. To appear in Journal of Coastal Eng.

Reniers, A.J.H.M, J.A. Battjes, A. Falques and D.A. Huntley, 1996: A laboratory study on the shear instability of longshore currents. To appear in JGR.

Visser, P.J.,1984: Uniform longshore current measurements and calculations. Proc. 19th Int. Conf. Coastal Eng., Houston, pp. 2192-2207.